Supporting Information

Three-Dimensional Porous Platinum-Tellurium-Rhodium Surface/Interface Achieve Remarkable Operating Fuel Cell Catalysis

Lingzheng Bu,[a,] Fandi Ning,[b] Jing Zhou,[c] Changhong Zhan,[a] Mingzi Sun,[d] Leigang Li,[a] Yiming Zhu,[e] Zhiwei Hu,[f] Qi Shao,[e] Xiaochun Zhou,[b] Bolong Huang,[d,]* and Xiaoqing Huang[a,]**

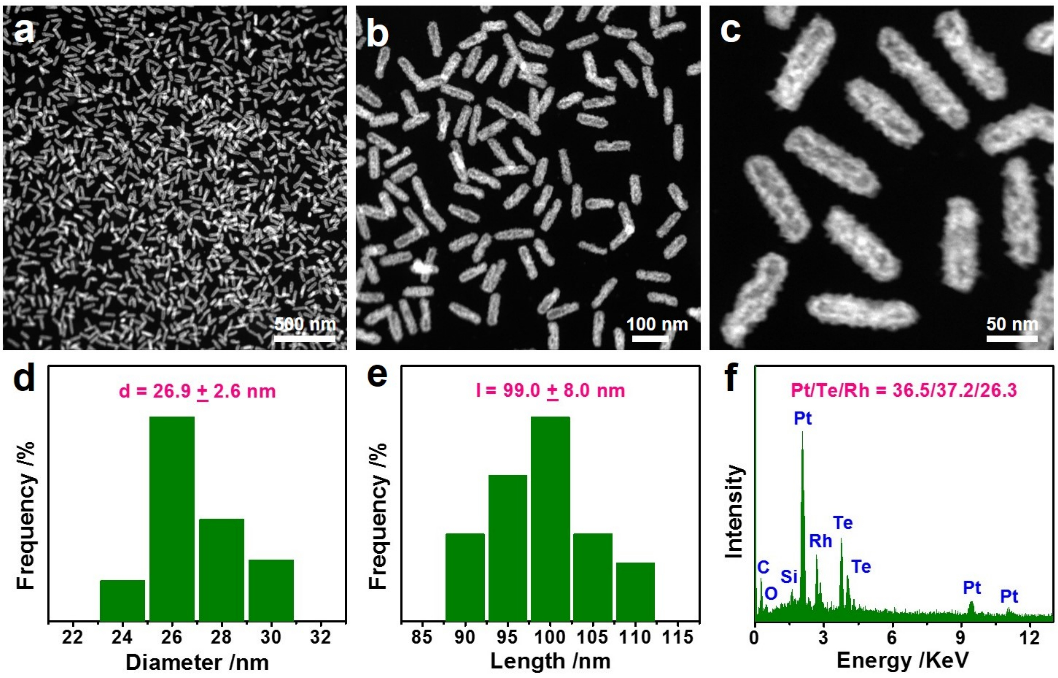

Figure S1. (a-c) HAADF-STEM images, (d) diameter distribution, (e) length distribution, and (f) SEM-EDS of $Pt_3Te_3Rh_2$ NRs.

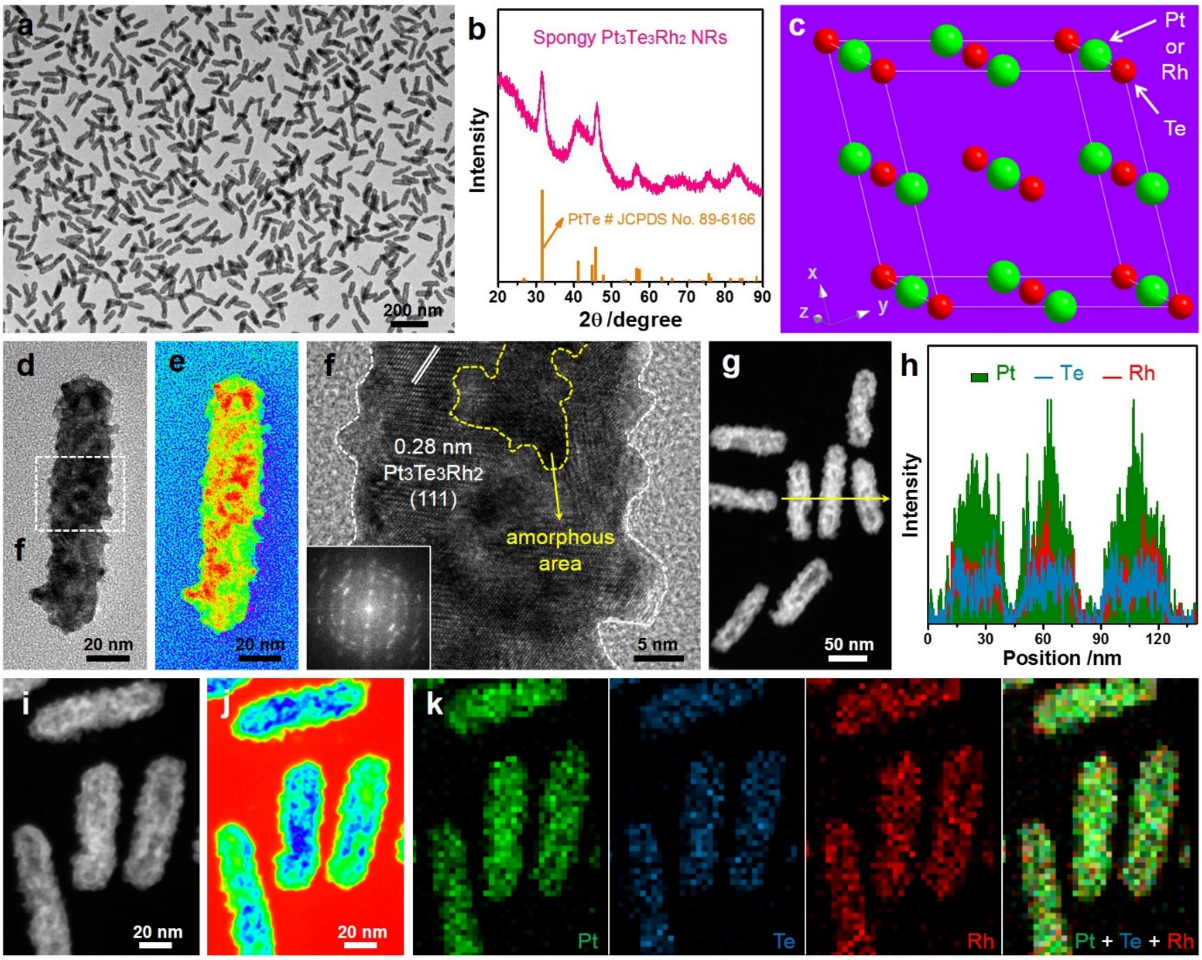

Figure S2. (a) TEM image, (b) PXRD pattern, (c) crystal structure, (d) enlarged TEM image and (e) corresponding rainbow-colored TEM image, (f) HRTEM image and related FFT pattern, (g) HAADF-STEM image and (h) corresponding line-scans, (i) HAADF-STEM image and (j) corresponding rainbow-colored HAADF-STEM image, and (k) HAADF-STEM-EDS elemental mappings of $Pt_3Te_3Rh_2$ NRs. The equalized rainbow colors ranging from red (high) to green (low) in (e) and the equalized rainbow colors ranging from blue (high) to yellow (low) in (j) obviously display the thickness difference of $Pt_3Te_3Rh_2$ NRs. The white and yellow dotted lines in (f) clearly reveal the presence of uneven surface and partially amorphized area for $Pt_3Te_3Rh_2$ NRs, respectively.

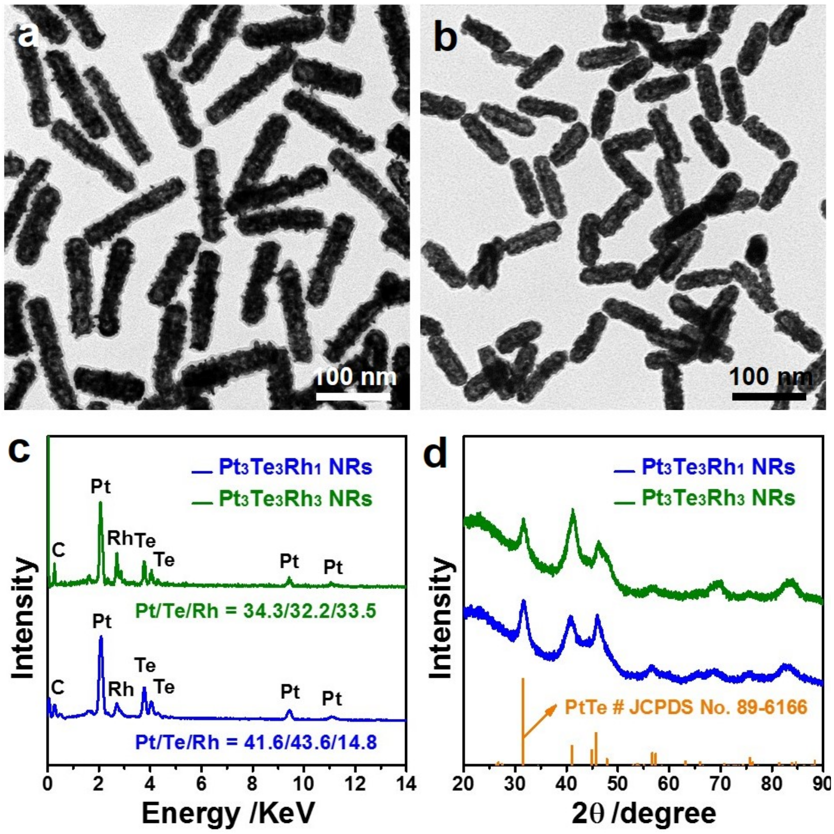

Figure S3. TEM images of (a) $Pt_3Te_3Rh_1$ NRs and (b) $Pt_3Te_3Rh_3$ NRs. (c) SEM-EDS and (d) PXRD patterns of $Pt_3Te_3Rh_1$ NRs and $Pt_3Te_3Rh_3$ NRs.

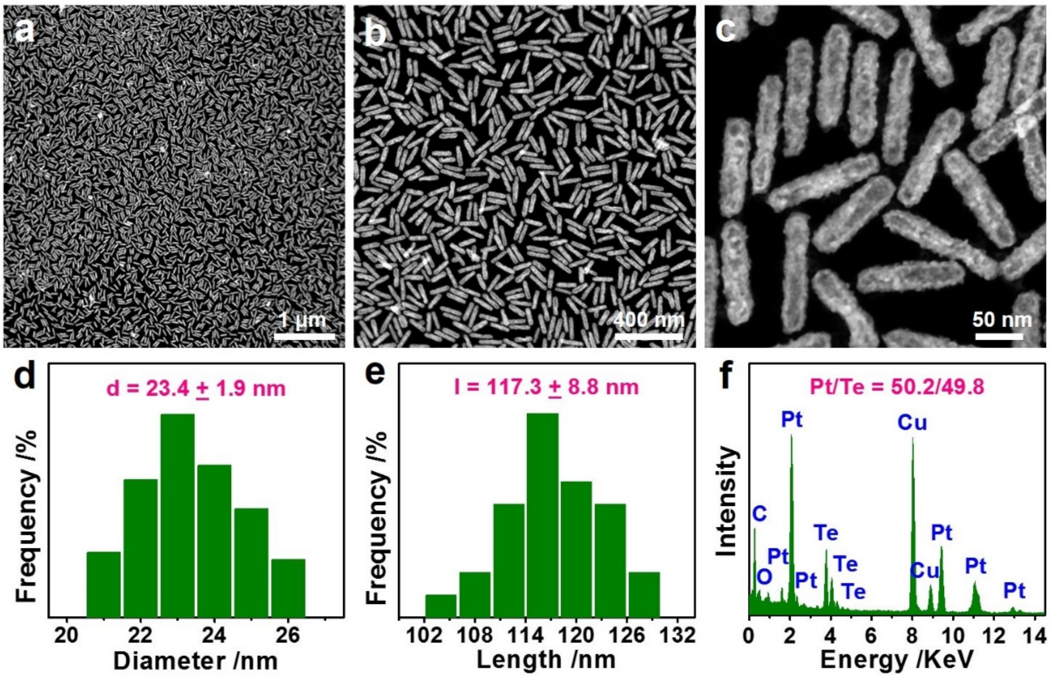

Figure S4. (a-c) HAADF-STEM images, (d) diameter distribution, (e) length distribution, and (f) TEM-EDS of PtTe NRs.

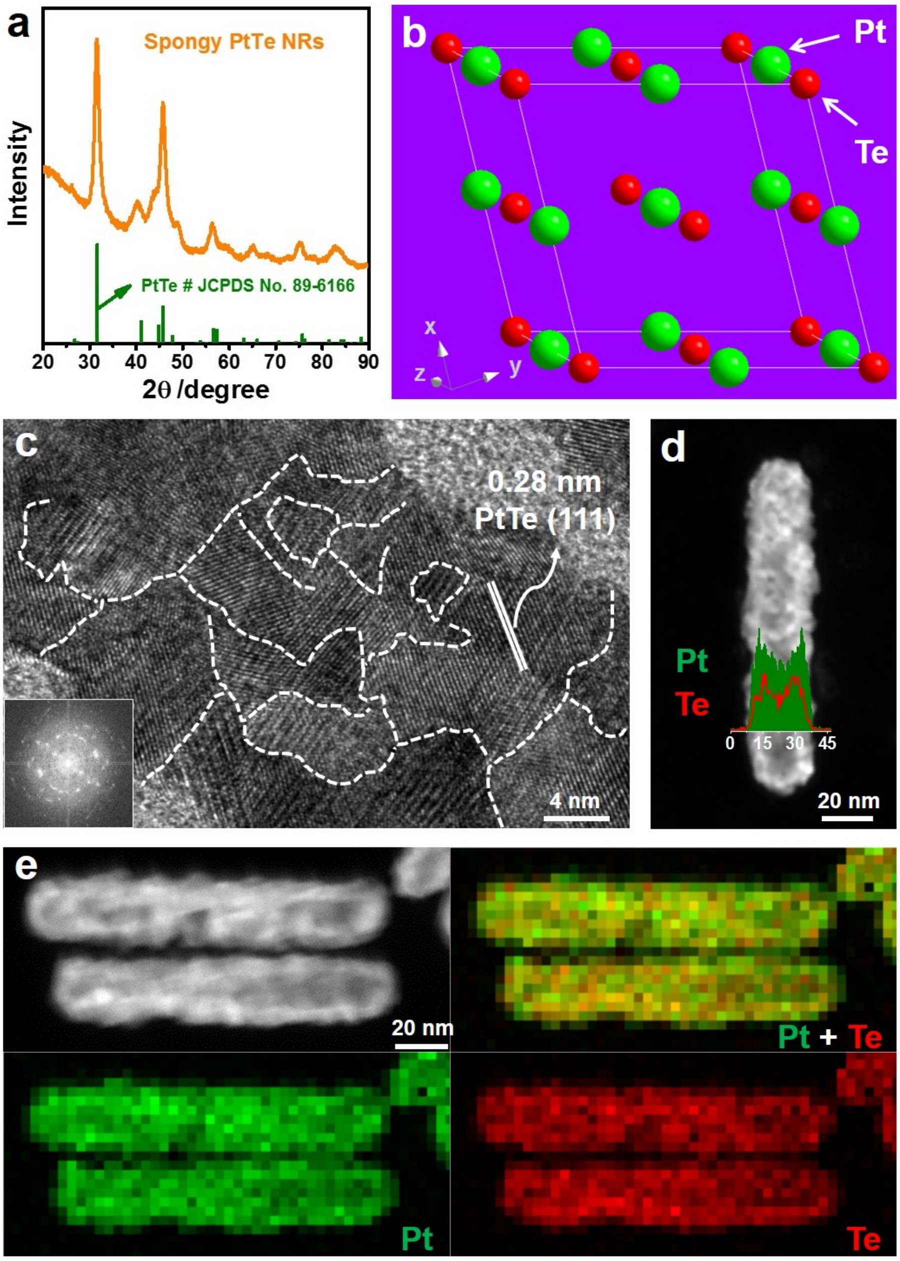

Figure S5. (a) PXRD pattern, (b) crystal structure, (c) HRTEM image and related FFT pattern, (d) HAADF-STEM image and corresponding line-scans, and (e) HAADF-STEM-EDS elemental mappings of PtTe NRs. The white dotted lines in (c) clearly reveal the presence of irregular facet boundaries.

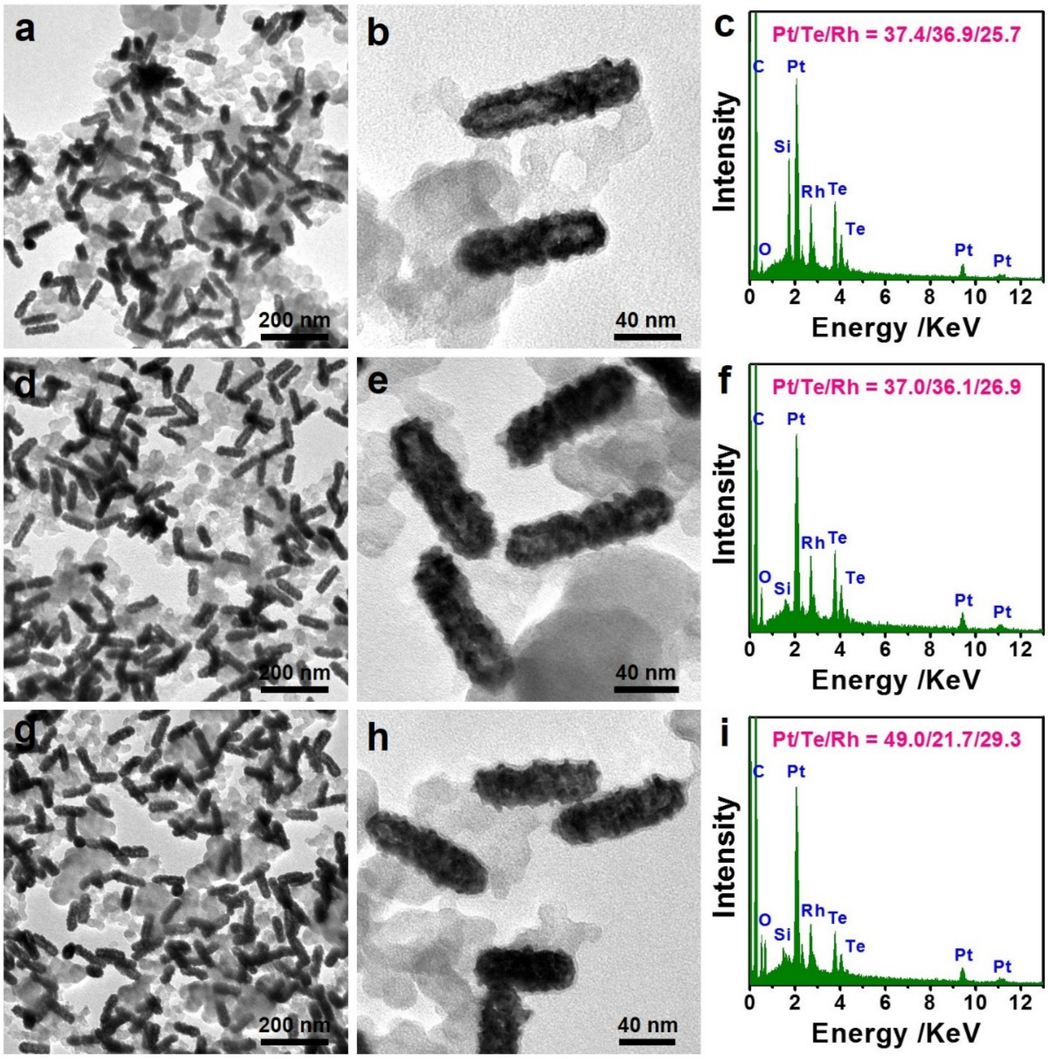

Figure S6. (a, b) TEM images and (c) SEM-EDS of initial $Pt_3Te_3Rh_2$ NRs/C. (d, e) TEM images and (f) SEM-EDS of $Pt_3Te_3Rh_2$ NRs/C after HAc washing. (g, h) TEM images and (i) SEM-EDS of $Pt_3Te_3Rh_2$ NRs/C after HAc washing and further annealing at 200 ^{o}C in air atmosphere for 1 h.

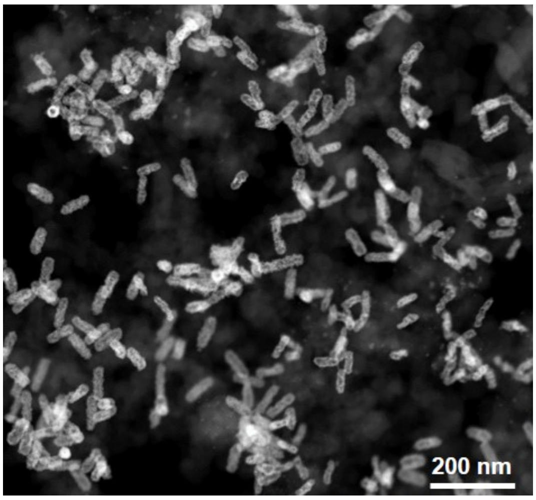

Figure S7. HAADF-STEM image of porous $Pt_{61}Te_{8}Rh_{31}$ NRs/C.

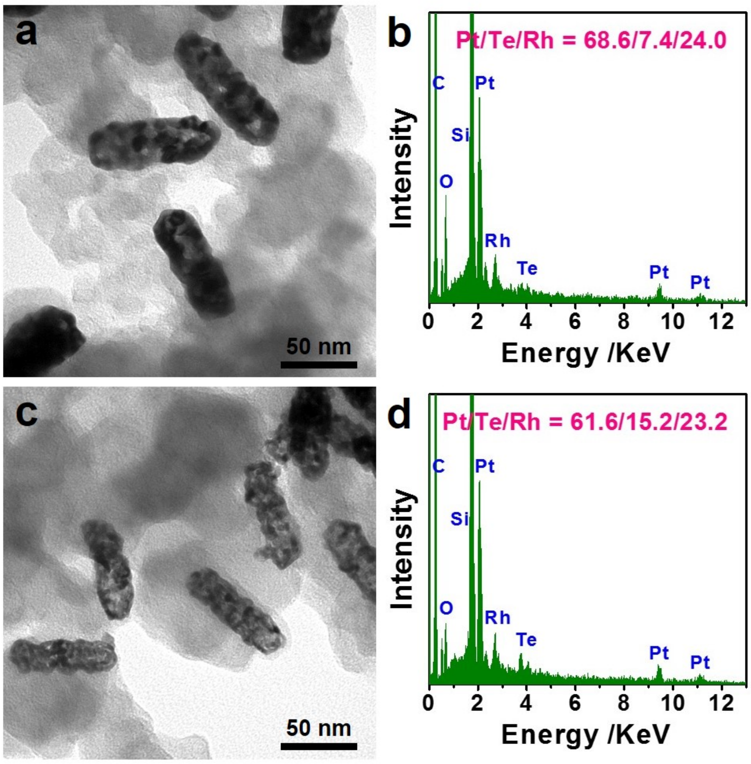

Figure S8. (a) TEM image and (b) SEM-EDS of porous $Pt_{69}Te_{7}Rh_{24}$ NRs/C. (c) TEM image and (d) SEM-EDS of porous $Pt_{62}Te_{15}Rh_{23}$ NRs/C.

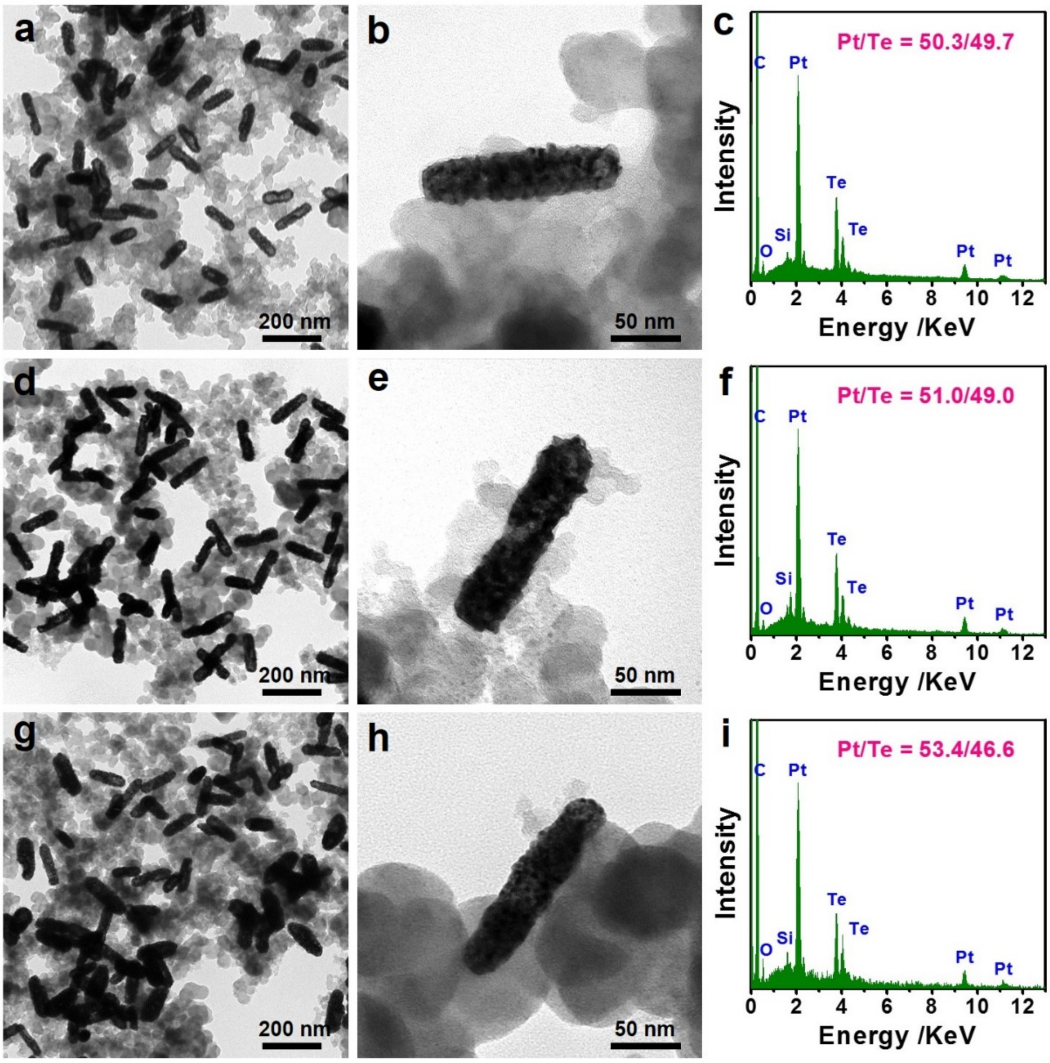

Figure S9. (a, b) TEM images and (c) SEM-EDS of initial PtTe NRs/C. (d, e) TEM images and (f) SEM-EDS of PtTe NRs/C after HAc washing. (g, h) TEM images and (i) SEM-EDS of PtTe NRs/C after HAc washing and further annealing at 200 ^{o}C in air atmosphere for 1 h.

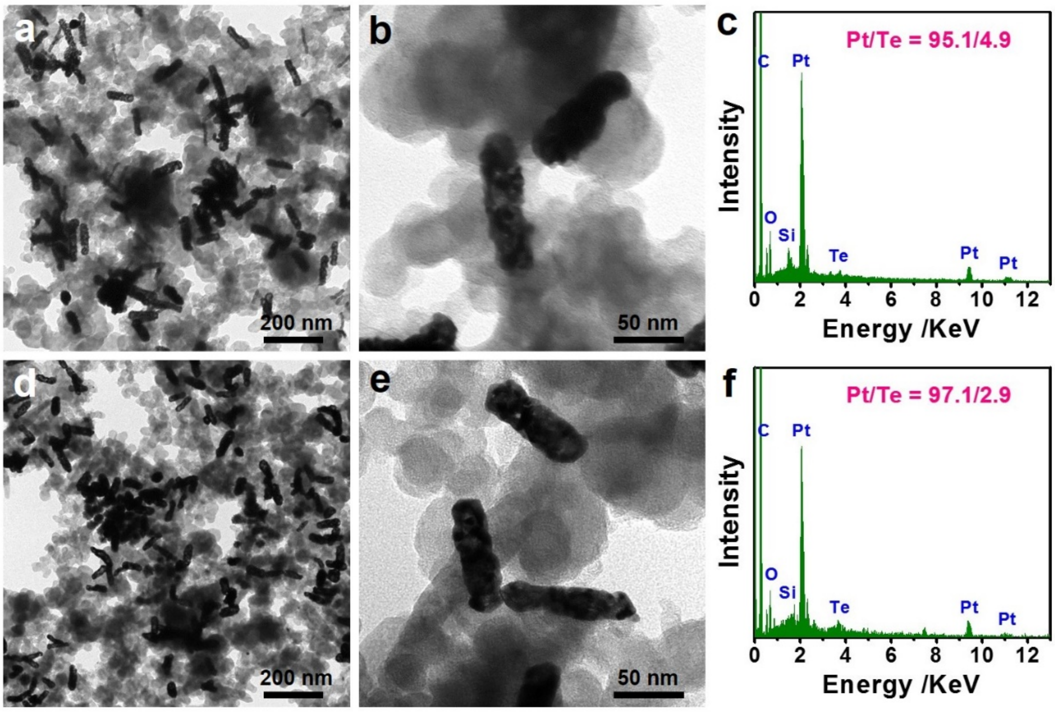

Figure S10. (a, b) TEM images and (c) SEM-EDS of PtTe NRs/C after HAc washing and further annealing at 200 ^{o}C in air atmosphere for 1 h and then electrochemical sweeping in 0.1 M $HClO_4$ solution for 1000 CV cycles (i.e. porous $Pt_{95}Te_5$ NRs/C). (d, e) TEM images and (f) SEM-EDS of porous $Pt_{95}Te_5$ NRs/C after 30000 potential cycles between 0.6 V and 1.1 V vs. RHE.

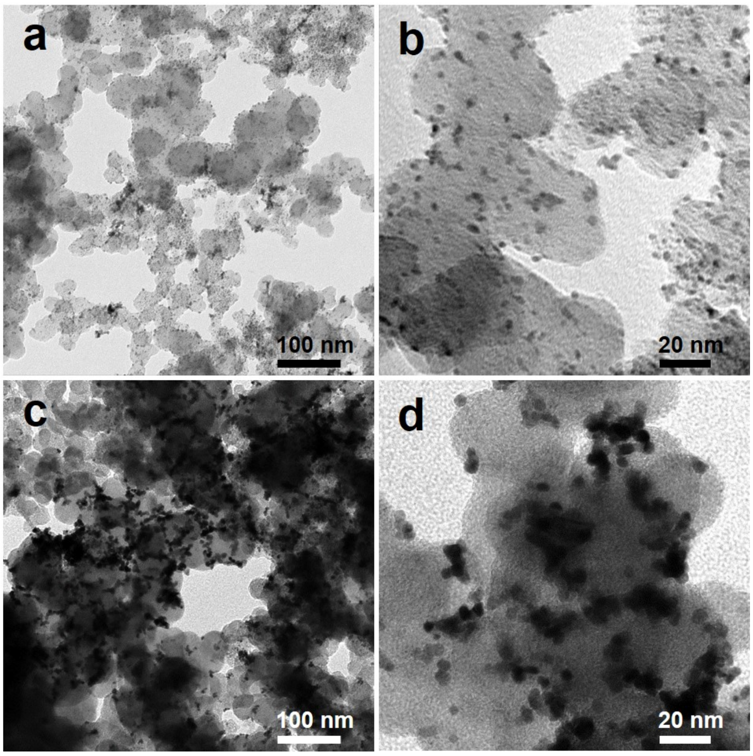

Figure S11. TEM images of commercial Pt/C (a, b) before and (c, d) after 30000 potential cycles between 0.6 and 1.1 V *vs.* RHE.

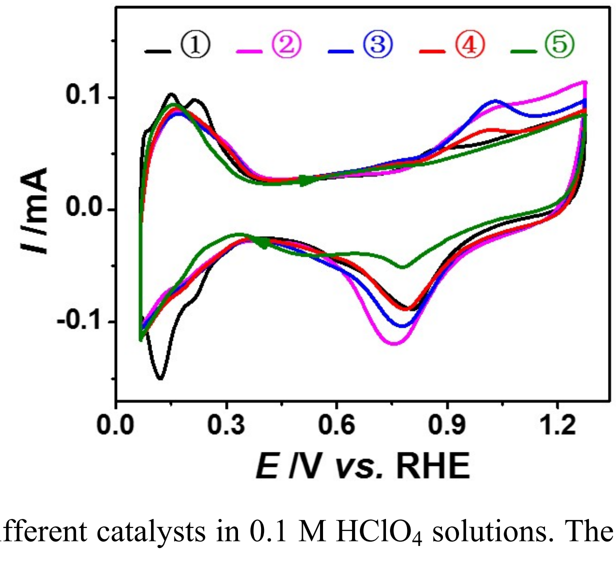

Figure S12. CVs of different catalysts in 0.1 M $HClO_4$ solutions. The colored symbols of ①, ②, ③, ④, and ⑤ represent commercial Pt/C, porous $Pt_{95}Te_5$ NRs/C, porous $Pt_{69}Te_7Rh_{24}$ NRs/C, porous $Pt_{61}Te_8Rh_{31}$ NRs/C, and porous $Pt_{62}Te_{15}Rh_{23}$ NRs/C, respectively.

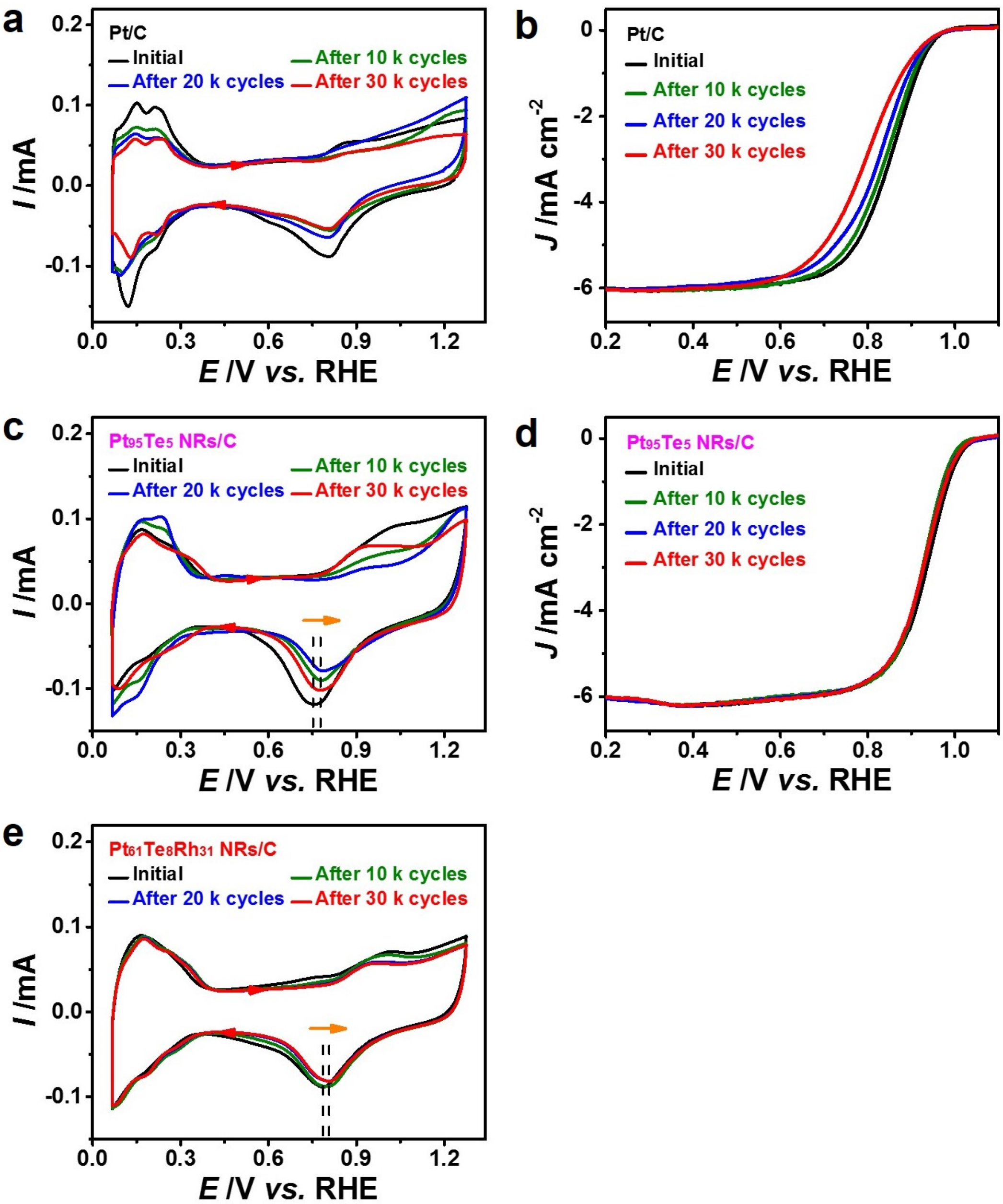

Figure S13. (a) CVs and (b) ORR polarization curves of commercial Pt/C before and after different potential cycles between 0.6 and 1.1 V *vs*. RHE. (c) CVs and (d) ORR polarization curves of porous $Pt_{95}Te_5$ NRs/C before and after different potential cycles between 0.6 and 1.1 V *vs*. RHE. (e) CVs of porous $Pt_{61}Te_8Rh_{31}$ NRs/C before and after different potential cycles between 0.6 and 1.1 V *vs*. RHE.

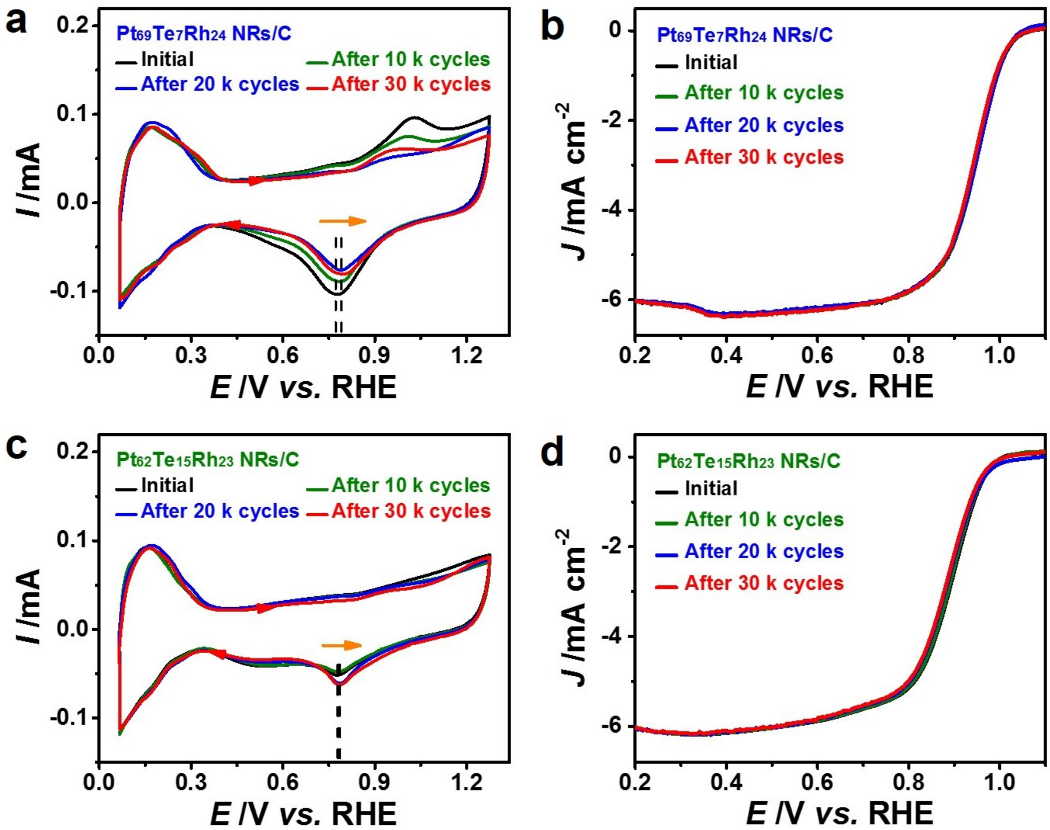

Figure S14. (a) CVs and (b) ORR polarization curves of porous $Pt_{69}Te_7Rh_{24}$ NRs/C before and after different potential cycles between 0.6 and 1.1 V *vs*. RHE. (c) CVs and (d) ORR polarization curves of porous $Pt_{62}Te_{15}Rh_{23}$ NRs/C before and after different potential cycles between 0.6 and 1.1 V *vs*. RHE.

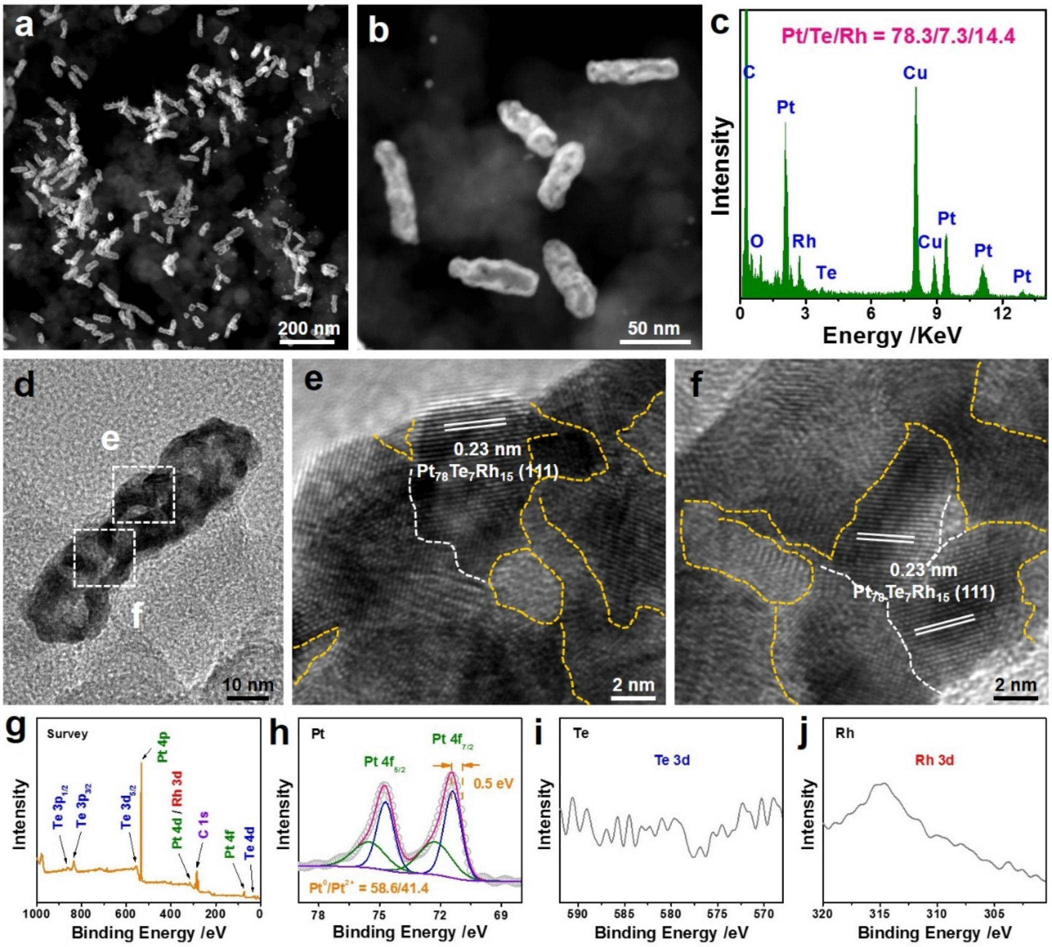

Figure S15. (a, b) HAADF-STEM images, (c) TEM-EDS, (d) TEM image, and (e, f) HRTEM images of porous $Pt_{61}Te_8Rh_{31}$ NRs/C after 30000 potential cycles between 0.6 and 1.1 V *vs.* RHE. The white and yellow dotted lines in (e, f) clearly reveal the presence of irregular facet boundaries and partially amorphized areas, respectively, further demonstrating the structure stability of porous $Pt_{61}Te_8Rh_{31}$ NRs/C in ORR medium. (g) Energy survey, (h) Pt 4f, (i) Te 3d, and (j) Rh 3d XPS spectra of porous $Pt_{61}Te_8Rh_{31}$ NRs/C after 30000 potential cycles between 0.6 and 1.1 V *vs.* RHE. The surface molar ratio of Pt/Te/Rh was 80.4/5.9/13.7 for porous $Pt_{61}Te_8Rh_{31}$ NRs/C after 30000 potential cycles between 0.6 and 1.1 V *vs.* RHE, as determined by the XPS.

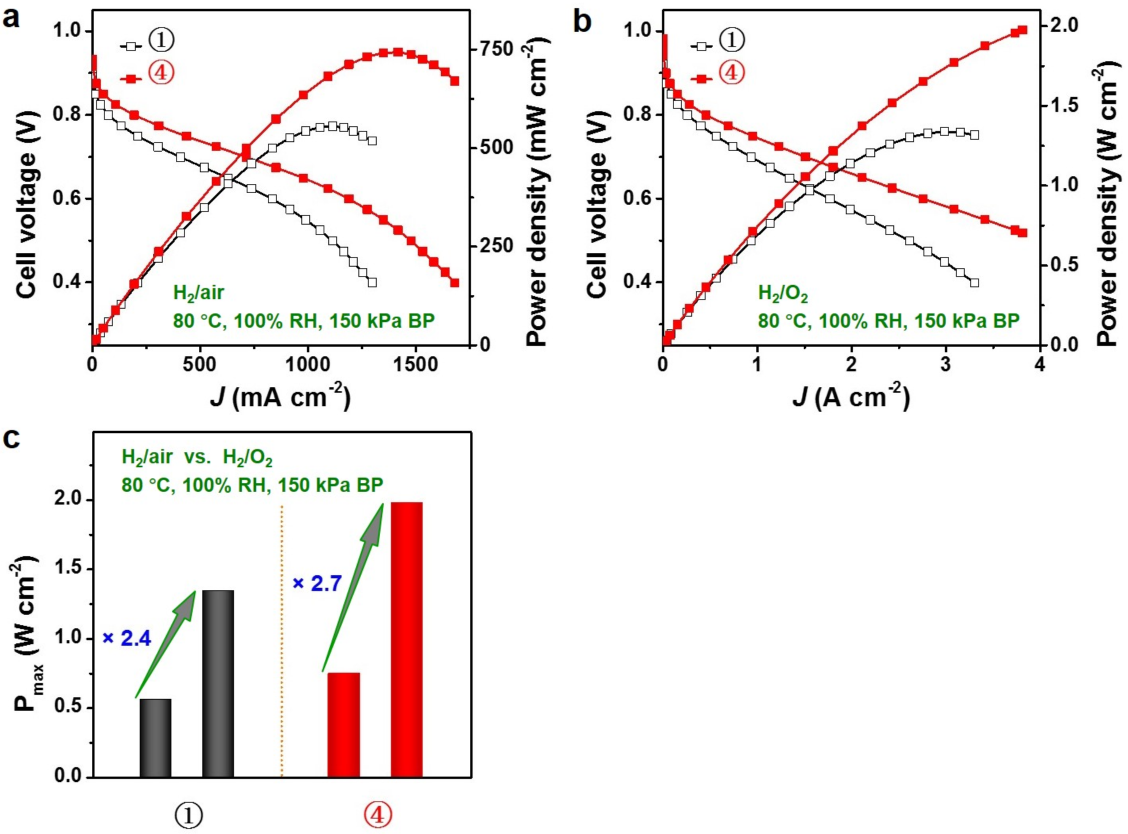

Figure S16. PEMFC polarization curves and power density curves of different cathodic catalysts in (a) H_2/air and (b) H_2/O_2 media at 150 kPa BP. (c) Histogram of maximum power densities for different catalysts in H_2/air and H_2/O_2 media at 150 kPa BP. The colored symbols of ① and ④ represent commercial Pt/C and porous $Pt_{61}Te_8Rh_{31}$ NRs/C, respectively.

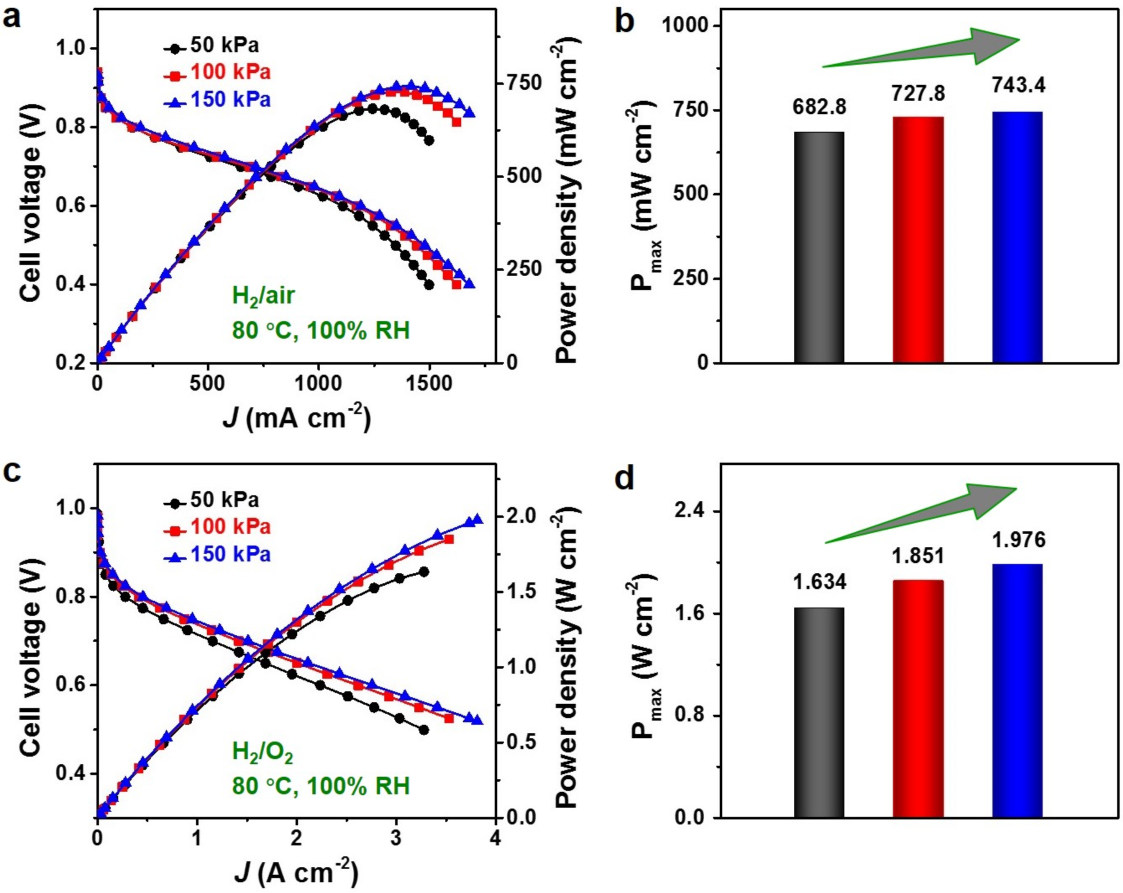

Figure S17. PEMFC polarization curves and power density curves of porous $Pt_{61}Te_8Rh_{31}$ NRs/C in (a) H_2/air and (c) H_2/O_2 media at 50/100/150 kPa BP. Histogram of maximum power densities for porous $Pt_{61}Te_8Rh_{31}$ NRs/C in (b) H_2/air and (d) H_2/O_2 media at 50/100/150 kPa BP.

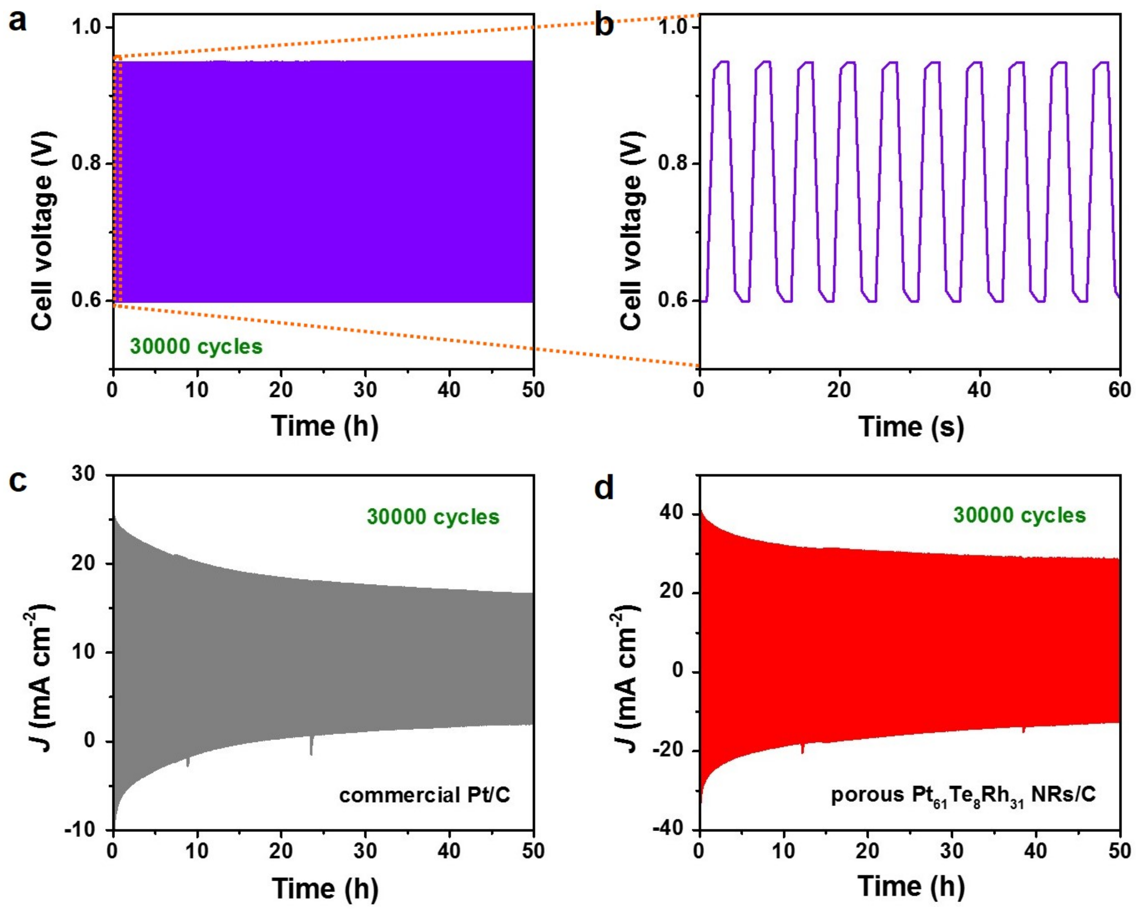

Figure S18. (a) The AST and (b) enlarged initial 60 s AST characterizations by square wave between 0.6 and 0.95 V at 3 s at each potential for 30000 cycles. The time-dependent current density curves of (c) commercial Pt/C and (d) porous $Pt_{61}Te_{8}Rh_{31}$ NRs/C during the AST for 30000 cycles. The AST was run at 200/200 mL min^{-1} H_2/N_2, 80/80 °C, 100/100% RH and 100/100 kPa BP in the order of anode/cathode.

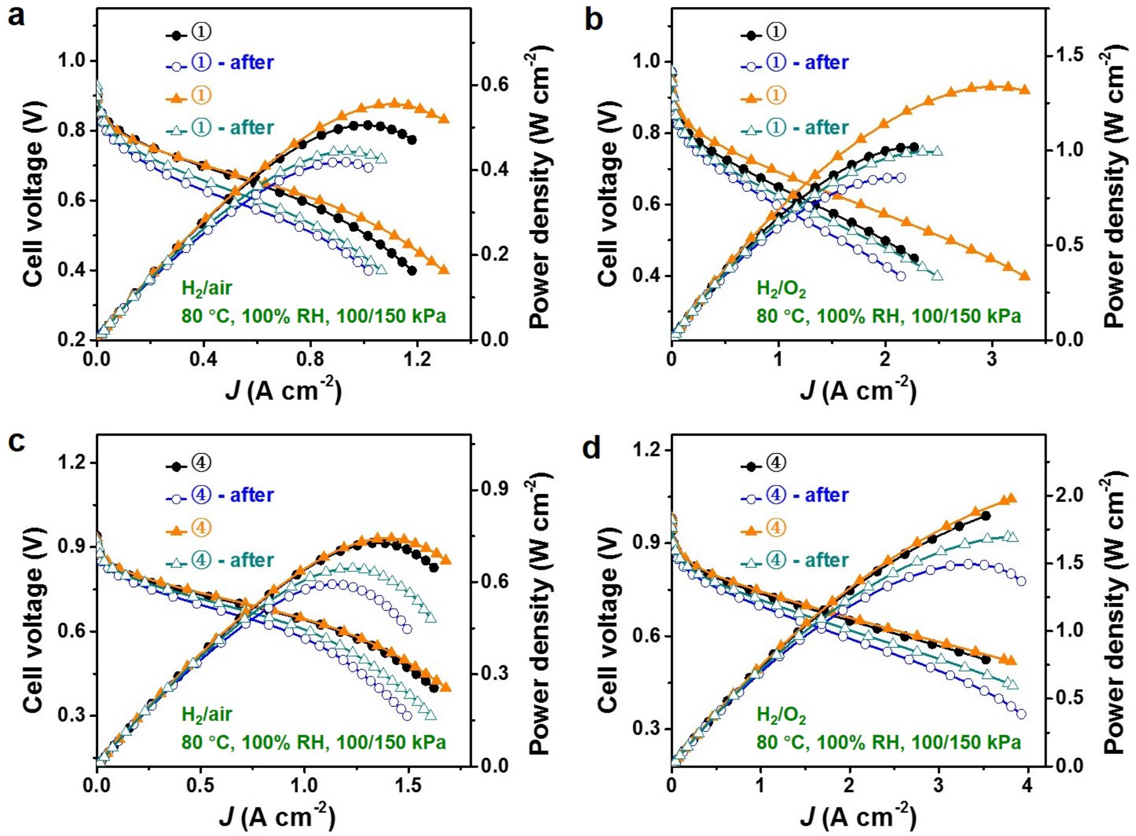

Figure S19. PEMFC polarization curves and power density curves of different cathodic catalysts before and after 30000 cycles at 100/150 kPa BP in (a, c) H_2/air and (b, d) H_2/O_2 media. The colored symbols of ① and ④ represent commercial Pt/C and porous $Pt_{61}Te_8Rh_{31}$ NRs/C, respectively.

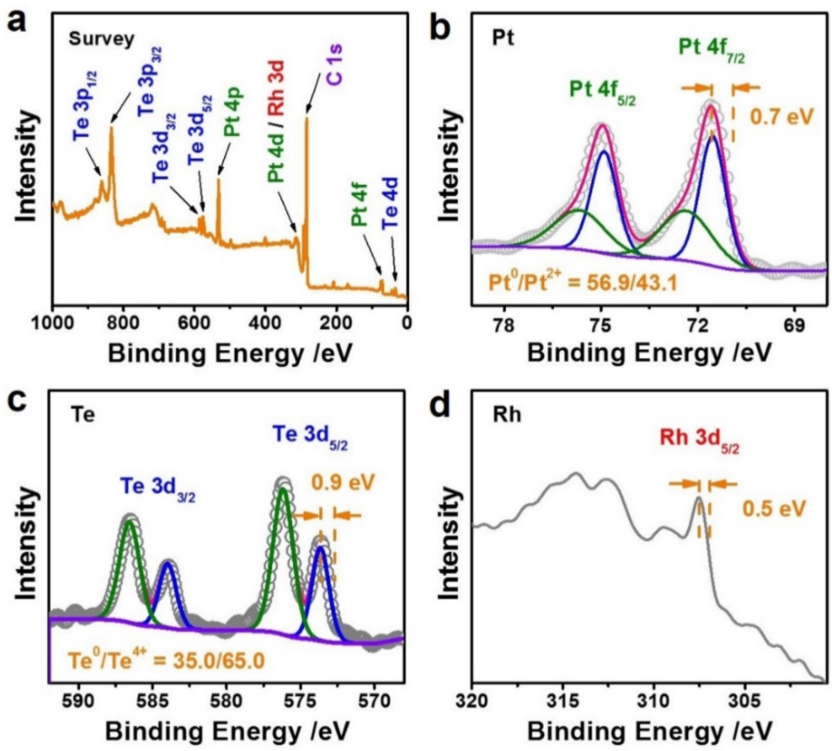

Figure S20. (a) Energy survey, (b) Pt 4f, (c) Te 3d, and (d) Rh 3d XPS spectra of initial $Pt_3Te_3Rh_2$ NRs/C. The surface molar ratio of Pt/Te/Rh was 36.2/36.1/27.7 for initial $Pt_3Te_3Rh_2$ NRs/C, as determined by the XPS.

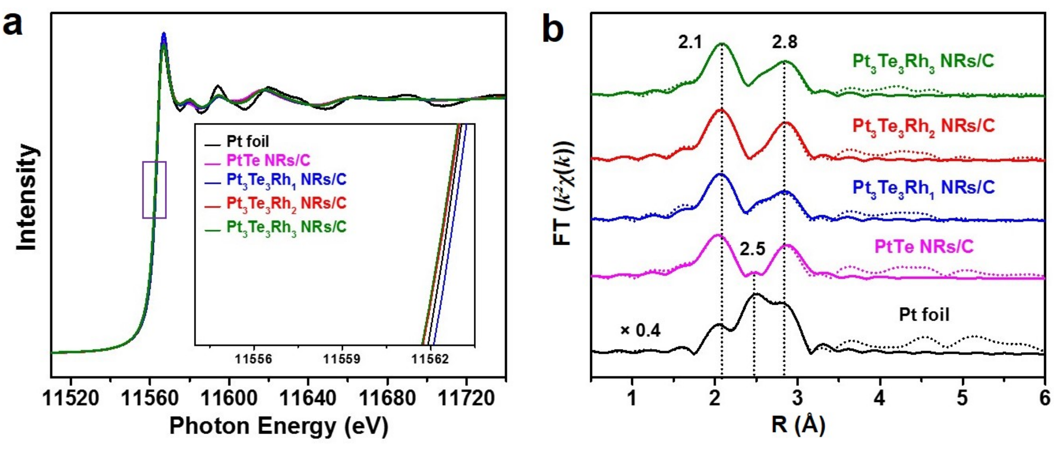

Figure S21. (a) Pt L_3-edge XANES profiles of Pt foil, PtTe NRs/C, and PtTeRh NRs/C with different compositions. The inset in (a) is the magnified near-edge structures of different catalysts. (b) Pt L_3-edge EXAFS spectra in R space for Pt foil, PtTe NRs/C, and PtTeRh NRs/C with different compositions. The dotted lines indicate the experiment data, and the solid lines represent the simulation data.

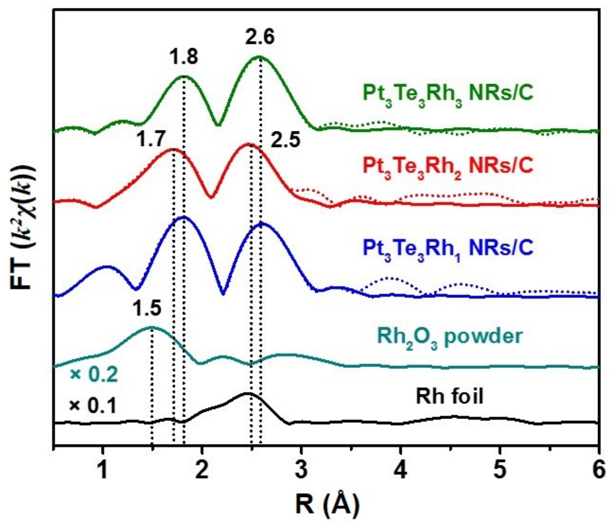

Figure S22. Rh K-edge EXAFS spectra in R space for Rh foil, Rh_2O_3 powder, and PtTeRh NRs/C with different compositions. The dotted lines indicate the experiment data, and the solid lines represent the simulation data.

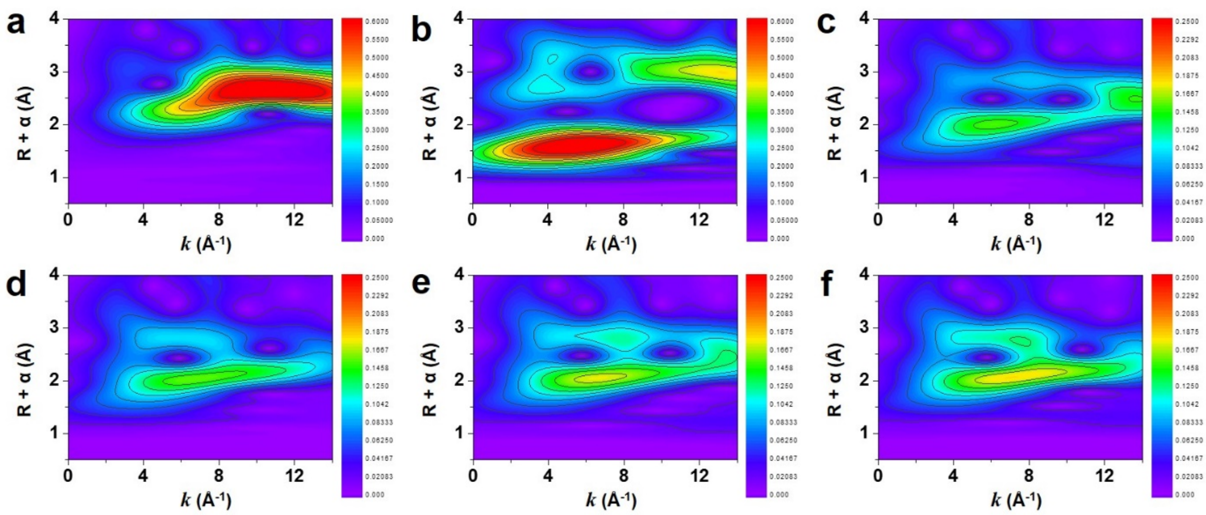

Figure S23. Wavelet transform analyses of the Pt L_3-edge EXAFS data for (a) Pt foil, (b) PtO_2, (c) PtTe NRs/C, (d) $Pt_3Te_3Rh_1$ NRs/C, (e) $Pt_3Te_3Rh_2$ NRs/C, and (f) $Pt_3Te_3Rh_3$ NRs/C.

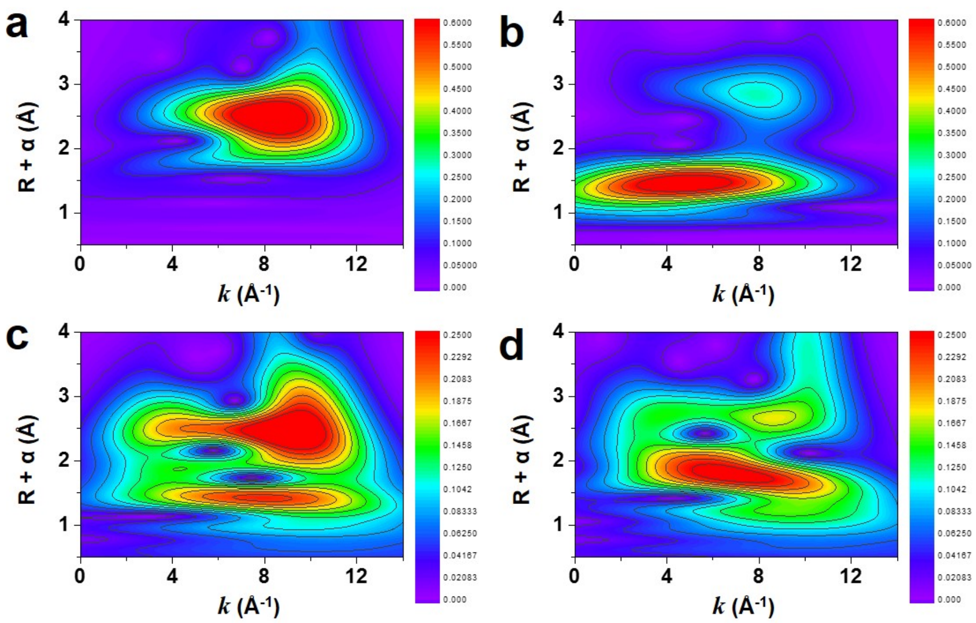

Figure S24. Wavelet transform analyses of the Rh K-edge EXAFS data for (a) Rh foil, (b) Rh_2O_3 powder, (c) $Pt_3Te_3Rh_2$ NRs/C, and (f) porous $Pt_{61}Te_8Rh_{31}$ NRs/C.

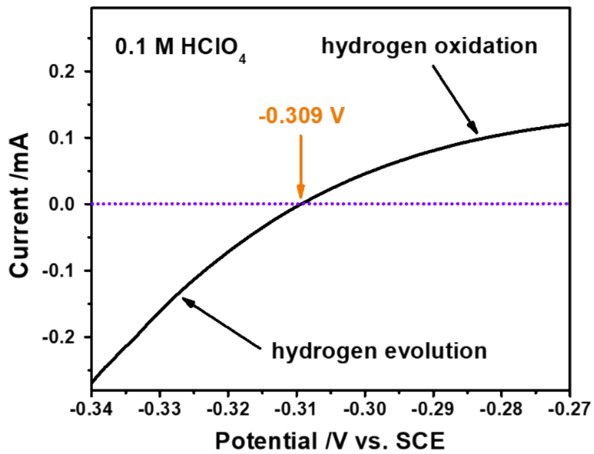

Figure S25. Calibration of SCE and conversion to RHE. The reference electrode calibration of SCE was performed in a standard three-electrode system with polished Pt plates (1 × 1 cm^2) as the working and counter electrodes, and the SCE as the reference electrode. The electrolyte was pre-purged and saturated with high purity H_2. Linear scanning voltammetry (LSV) was then run at a scan rate of 0.1 mV s^{-1}, and the potential at which the current crossed zero was taken to be the thermodynamic potential (*vs.* SCE) for the hydrogen electrode reaction. In the 0.1 M $HClO_4$ solution, the zero current point was at -0.309 V *vs.* SCE, so E (RHE) = E (SCE) + 0.309 V.

Table S1. ECSAs and ORR activities of different catalysts at 0.90 V *vs.* RHE. ORR measurements were performed at room temperature in O_2-saturated $HClO_4$ solution at a sweep rate of 10 mV s^{-1} and a rotation rate of 1600 rpm. The activities were calculated based on several parallel measurements after Ohmic drop correction.

Catalyst	**Loading of metal Pt (μg)**	**ECSA (m^2 g^{-1})**	**Mass activity at RT (A mg^{-1}_{Pt})**	**Specific activity at RT (mA cm^{-2})**
commercial Pt/C	2.0	68.9	0.17	0.25
porous $Pt_{95}Te_5$ NRs/C	2.0	52.7	1.41	2.68
porous $Pt_{69}Te_7Rh_{24}$ NRs/C	2.0	53.5	2.05	3.83
porous $Pt_{61}Te_8Rh_{31}$ NRs/C	2.0	54.3	2.40	4.42
porous $Pt_{62}Te_{15}Rh_{23}$ NRs/C	2.0	54.1	0.42	0.78

Table S2. Acidic ORR activities of porous $Pt_{61}Te_8Rh_{31}$ NRs/C and state-of-the-art Pt-based nanocatalysts from recent 5 years-published works at 0.90 V/0.95 V *vs.* RHE. The ORR measurements were performed at room temperature in O_2-saturated $HClO_4$ solution at a sweep rate of 10 mV s^{-1} and a rotation rate of 1600 rpm.

Catalyst	J_m (A mg^{-1}_{Pt})	J_s (mA cm^{-2})	Ref.
Porous $Pt_{61}Te_8Rh_{31}$ NRs/C	**2.40/1.22 @ 0.90 V/0.95 V *vs.* RHE**	**4.42/2.24 @ 0.90 V/0.95 V *vs.* RHE**	**This Work**
Porous $Pt_{61}Te_8Rh_{31}$ NRs/C-ADT	**2.22/0.59 @ 0.90 V/0.95 V *vs.* RHE**	**3.99/1.06 @ 0.90 V/0.95 V *vs.* RHE**	
PtCu Octopod Nanoframes/C	3.26	5.98	*Adv. Mater.* **2017**, *29*, 1601687
PtCuBiMn Nanosheets/C	0.69	2.41	*Adv. Mater.* **2017**, *29*, 1604994
Pt Nanowires/C	0.71	2.20	*Adv. Mater.* **2017**, *29*, 1703460
$Pt_{1.3}Ni$ Nanowires/C	1.52	3.58	
Rh-Doped Pt Nanowires/C	1.41	1.63	*J. Am. Chem. Soc.* **2017**, *139*, 8152
$PtPb_{1.12}Ni_{0.14}$ Octahedra/C	1.92	5.16	*J. Am. Chem. Soc.* **2017**, *139*, 9576
PtCo@HGS	0.97	0.92	*Adv. Energy Mater.* **2017**, *7*, 1700835
Pt-Ni Nanocage/C	0.50	0.70	*Appl. Catal. B: Environ.* **2017**, *203*, 927
PtCuPd Cubic Nanoskeletons/C	1.04	2.41	*Nano Energy* **2017**, *39*, 532
PtCo Excavated Octahedra/C	~ 0.35	1.85	*Nano Energy* **2017**, *39*, 582
Pt_2Co Excavated Octahedra/C	~ 0.32	2.41	
PtCu Dendrites@PtCuNi Frames/C	2.48	7.34	*ACS Nano* **2017**, *11*, 10844
Porous PtAgBiCo Nanoplates/C	0.81	1.95	*Chem. Sci.* **2017**, *8*, 4292
PtNi Nanoporous Nanowires/C	0.33	0.99	*J. Mater. Chem. A* **2017**, *5*, 23651
RD-CuPt Nanoframes/C	0.92	1.70	*Chem. Mater.* **2017**, *29*, 5681
Spiny RD-CuPt Nanoframes/C	0.86	2.19	
B-Doped Pt_3Ni Nanoparticles/C	0.60	1.35	*Electrochim. Acta* **2017**, *246*, 242
Pt_3Ni Nanoparticles/C	0.35	1.00	
Pt Nanoparticles/C	0.20	0.23	
$L1_2$-Pt_3Fe Nanoparticles/C	0.45	1.36	*ACS Appl. Mater. Interfaces* **2017**, *9*, 31806
Pt-Fe Nanoparticles/C	0.19	0.51	
PtCo Concave Nanocubes/C	0.24	0.44	*ACS Appl. Mater. Interfaces* **2017**, *9*, 36164
PtCo+Co@Graphene+Co-N_x-C_y	8.64/2.68	7.86/2.44	*Science* **2018**, *362*, 1276
Pt_3Co+Co@Graphene+Co/Zn-N_x-C_y	12.36/3.95	10.66/3.41	
Pt_3Co/ZC	2.98/0.91	NA	
$L1_0$-FePt/Pt Nanoparticles/C	0.70	NA	*J. Am. Chem. Soc.* **2018**, *140*, 2926
Pt Nanowires/C	0.88	1.23	*J. Am. Chem. Soc.* **2018**, *140*, 16159
Pt_3Ni Nanowires/C	2.10	2.34	
$Pt_3NiRh_{0.26}$ Nanowires/C	2.88	2.71	
Pt-Skin Pt_3Fe z-Nanowires/C	2.11	4.34	*Adv. Mater.* **2018**, *30*, 1705515
Pt_3Fe z-Nanowires/C	1.11	2.06	
Rhombic Dodecahedral PtCuCo Nanoskeletons/C	1.56	2.69	*Adv. Funct. Mater.* **2018**, *28*, 1706440
Ga-Doped PtNi Octahedra/C	1.24	2.53	*Nano Lett.* **2018**, *18*, 2450

Pt Nanoparticles/40Co-NC-900	~ 0.25	1.15	*Nano Lett.* **2018**, *18*, 4163
Ultrathin Pt Nanoplates/C	1.62	5.30	*Chem. Sci.* **2018**, *9*, 398
Pt_3Ni(Pt-skin)/Pd_{20} Nanoparticles/C	14.20	16.70	*Chem. Sci.* **2018**, *9*, 6134
PtCo/Co@NHPCC	0.57	NA	*Appl. Catal. B.* **2018**, *225*, 496
Pt-o-Cu_3Pt Nanoparticles/C	0.64	1.73	*ACS Appl. Mater. Interfaces* **2018**, *10*, 38015
Pt-d-Cu_3Pt Nanoparticles/C	0.57	1.32	
Rhombic Dodecahedral PtCuNi Nanoskeletons/C	0.86	1.65	*J. Power Sources* **2018**, *406*, 42
PtCu Dodecahedral Nanoskeletons/C	0.79	2.03	*Chemcatchem* **2018**, *10*, 931
Pt-Ni Bunched Nanocages/C	3.52	5.16	*Science* **2019**, *366*, 850
Pt-Ni Bunched Nanospheres/C	1.89	4.34	
Pt Nanowires/C	1.02	2.20	
$L1_0$-CoPt/Pt Nanoparticles/C	2.26	8.26	*Joule* **2019**, *3*, 124
Etched A1-CoPt Nanoparticles/C	0.15	0.70	
SnO_x/Pt-Cu-Ni (5) Nanoparticles/C	NA	1.60	*J. Am. Chem. Soc.* **2019**, *141*, 9463
$Pt_{4.31}Ga$ Nanowires/C	1.89	3.28	*J. Am. Chem. Soc.* **2019**, *141*, 18083
C-$L1_0$-$PtNi_{0.8}Co_{0.2}$ Nanoparticles	2.28	4.38	*Adv. Energy Mater.* **2019**, *9*, 1803771
H-PtCo@Pt_1N-C	1.20	2.39	*Adv. Funct. Mater.* **2019**, *29*, 1807340
Ordered $PtCo_3$ H600	0.72	NA	*Adv. Funct. Mater.* **2019**, *29*, 1902987
$L1_0$-W-PtCo Nanoparticles/C	2.21	3.60	*Angew. Chem. Int. Ed.* **2019**, *58*, 15471
$L1_0$-PtCo Nanoparticles/C	1.17	1.92	
Pt Nanoplates/C	3.43	5.76	*Nano Lett.* **2019**, *19*, 3730
4.6%Pd-Doped Pt Nanoplates/C	~ 3.79	6.01	
Pt/Se Nanoparticles/C	0.75	0.32	*Nano Lett.* **2019**, *19*, 4997
Pt_2Ni_2 Nanoparticles/C	0.89	2.31	*ACS Catal.* **2019**, *9*, 11431
$Pt_2In_{0.2}Ni_{1.8}$ Nanoparticles/C	0.76	1.96	
$Pt_2In_1Ni_1$ Nanoparticles/C	0.27	0.60	
5 nm-Pt Nanoparticles/C	0.09	0.18	*Chem. Mater.* **2019**, *31*, 8205
6.2 nm-Pt_2P Nanoparticles/C	0.92	1.86	
Pd@PtNi Nanowires/C	1.75	3.18	*Small* **2019**, *15*, 1900288
PdPtNi Nanoparticles/C	0.71	1.25	
PtNi Nanoparticles@C-2 Composites	0.84	1.54	*ACS Appl. Energy Mater.* **2019**, *2*, 2769
Pt_3Co Nanoparticles/C	~ 1.13	~ 2.25	*ACS Appl. Mater. Interfaces* **2019**, *11*, 26789
$Pt_{0.7}Fe_{0.3}$ Nanoparticles/C	0.17	0.25	*ACS Sustainable Chem. Eng.* **2019**, *7*, 6541
$Pt_{0.7}Co_{0.3}$ Nanoparticles/C	0.18	0.26	
$Pt_{0.7}Ni_{0.3}$ Nanoparticles/C	0.28	0.37	
$Pt_{0.78}Ni_{0.22}$ Rough Nanowires/C	1.07	1.02	*Nano Res.* **2019**, *12*, 1721
Pt Rough Nanowires/C	0.67	0.62	
37 wt%-FePt Nanoparticles/rGO	1.96	NA	*J. Am. Chem. Soc.* **2020**, *142*, 14190
V_{Cu}-PtCu Nanowire Networks	3.15	4.97	*Angew. Chem. Int. Ed.* **2020**, *59*, 13778
$L1_0$-PtZn Nanoparticles/C	1.02	1.68	*Adv. Energy Mater.* **2020**, *10*, 2000179
Pt-Co Concave Nanocubes@C	0.26	2.34	*ACS Appl. Energy Mater.* **2020**, *3*, 5077
Ordered PtCu Nanoskeletons/C	2.47	4.69	*Nano Lett.* **2020**, *20*, 7413

PtNi Nanoparticles/C-3.28	0.52	0.82	*ACS Appl. Mater. Interfaces* **2020**, *12*, 16286
Hollow PtNi Nanoparticles/C-2.60	0.75	1.16	
Hollow PtNi Nanoparticles/C-2.30	0.85	1.49	
Hollow PtNi Nanoparticles/C-2.05	0.62	1.19	
Pt_{ML}/Pd_{NS}/WNi/C	2.96	NA	*ACS Catal.* **2020**, *10*, 4290
Pt_{ML}/Pd_{NS}/C	2.53	NA	
Dealloyed 5.1 nm $PtCo_3$ Nanoparticles/C	NA	1.51	*ACS Catal.* **2020**, *10*, 4361
Int-PtNiN Nanoparticles/KB	1.83	2.92	*ACS Catal.* **2020**, *10*, 10637
D-PtNiN Nanoparticles/KB	0.58	1.25	
D-PtNi Nanoparticles/KB	0.46	1.10	
46.4% Commercial Pt/C TKK	0.18	0.38	
Pd@Pt Nanoparticles/C-As-Synthesized	0.99/0.10	NA	*ACS Catal.* **2020**, *10*, 14567
Pd@Pt Nanoparticles/C-As-Synthesized + Melamine	1.95/0.37	NA	
Pd@Pt Nanoparticles/C-After HAP	1.46/0.14	NA	
Pd@Pt Nanoparticles/C-After HAP + Melamine	3.63/0.54	NA	
Highly Distorted Pt Nanorods/C	2.77	4.70	*CCS Chem.* **2020**, *2*, 401
Weakly Distorted Pt Nanorods/C	0.49	1.02	
20% Commercial Pt/C JM	0.17	0.25	
Pt/PtP_2 Nanoparticles@NPC	0.72	0.51	*J. Mater. Chem. A* **2020**, *8*, 20463
PtP_2 Nanoparticles@NPC	0.47	0.44	
Pt Nanoparticles@NPC	0.15	0.18	
PtCo ERD Nanocrystals/C	0.94	2.68	*Nanoscale Adv.* **2020**, *2*, 4881
PtCo RD Nanocrystals/C	0.54	1.43	
N-Doped Pt Nanoparticles/C	0.102	0.148	*J. Catal.* **2020**, *382*, 247
N-Doped Pt Nanoparticles/C-H_2	0.096	0.146	
60% Commercial Pt/C JM	0.095	0.132	
Pt Nanoparticles/p-BN	1.06	1.24	*Chem. Eng. J.* **2020**, *399*, 125827
20% Commercial Pt/C HPT020	0.17	0.27	
PtFe/Pt-i-Nanoparticles/C	~ 2.20	~ 1.80	*Science* **2021**, *374*, 459
PtCo/Pt-i-Nanoparticles/C	~ 2.50	~ 2.75	
PtNi/Pt-i-Nanoparticles/C	~ 2.40	~ 3.30	
$PtCu_3$/Pt-i-Nanoparticles/C	4.18	3.80	
PtZn/Pt-i-Nanoparticles/C	~ 1.90	~ 1.20	
Pt-CoO 1 Network	4.60	4.57/0.52	*Nat. Mater.* **2021**, *20*, 208
Pt-CoO 2 Network	5.19	4.52/0.51	
Pt-CoO 3 Network	5.74	3.77/0.49	
Pt-CoO Heat 1 Network	6.75	4.59/0.59	
Pt-CoO Heat 2 Network	8.37	5.38/0.62	
$L1_2$-Pt_3Co Nanoparticles/FeN_4-C	1.34	3.98	*Energy Environ. Sci.* **2021**, *14*, 4948
Pt Nanoparticles/FeN_4-C	0.57	0.79	
Commercial Pt/C TKK-TEC10V20E	0.24	0.44	
PdPt Tesseracts/C	1.86	2.09	*J. Am. Chem. Soc.* **2021**, *143*, 496
Coplanar Pt/C NMs	1.01	NA	*Angew. Chem. Int. Ed.* **2021**, *60*, 6533
H-Pt Superstructures/C	2.24	4.52	*Nano Lett.* **2021**, *21*, 5075
M-Pt Superstructures/C	1.92	NA	

L-Pt Superstructures/C	0.77	NA	
Ru-Pt_3Co Octahedra/C	1.05	2.32	*Nano Lett.* **2021**, *21*, 6625
Pt_3Co Octahedra/C	1.07	2.16	
20% Commercial Pt/C JM	0.14	0.21	
1.1 nm-Pt Nanowires/C	1.00	1.20	*Nano Lett.* **2021**, *21*, 9354
1.5 nm-Pt Nanowires/C	0.77	0.95	
2.4 nm-Pt Nanowires/C	0.51	0.68	
20% Commercial Pt/C HISPEC3000	0.17	0.26	
Pt_{NS}-$PtNi_3$ Nanoparticles/C	4.40	9.08	*ACS Catal.* **2021**, *11*, 355
Pt_{NS}-Pt Nanoparticles/C	1.00	1.81	
20% Commercial Pt/C JM	0.14	0.20	
Pt_1@Pt/N-Doped Active Carbon	0.24	0.62	*ACS Catal.* **2021**, *11*, 466
Pt_1@Pt/Active Carbon	0.08	0.42	
20% Commercial Pt/C TKK	0.075	0.08	
PtFe@NC/SWCNHs (H_2-9 h)	1.53	3.61	*ACS Catal.* **2021**, *11*, 9355
Pt-Fe@NC/SWCNHs	0.75	1.92	
Pt@Co SAs-ZIF-NC	0.48	0.64	*Nano Energy* **2021**, *88*, 106221
20% Commercial Pt/C JM	0.16	0.21	
PtCoNi Nanoparticles@NCNTs	3.46	4.61	*Sci. Bull.* **2021**, *66*, 2207
h-PtNiCo Branched Nanocages/C	1.03	2.75	*J. Mater. Chem. A* **2021**, *9*, 23444
h-PtNi Branched Nanocages/C	0.37	1.39	
Pt_3Co@Pt Nanoparticles/C	0.71	2.75	*ChemCatChem* **2021**, *13*, 1587
700-Pt_1Co_1-IMC@Pt/C-2.5	0.53	1.11	*Energy Environ. Sci.* **2022**, *15*, 278
PtCo Nanoparticles@NGNS	1.29	1.70	*Angew. Chem. Int. Ed.* **2022**, *61*, e202115835
20% Commercial Pt/C	0.15	0.20	
PtCu Nested Skeleton Cubes/C	3.86	7.40	*Adv. Sci.* **2022**, *9*, 2104927
PtCu A-Nested Skeleton Cubes/C	5.13	7.20	
PtCu Octahedral Stars/C	0.59	1.70	
PtCu A-Octahedral Stars/C	1.02	2.14	
Pt-Skin $Pt_{78}Zn_{22}$ Nanocubes/KB	1.18	3.64	*Adv. Sci.* **2022**, *9*, 2200147
Pd@Pt_{3L} Nanoparticles/C	0.58	0.71	*Nano Res.* **2022**, *15*, 1892
PtFe (0.9) Nanoparticles/C	0.69	0.71	*Chem. Eng. J.* **2022**, *428*, 131569
PtFe (5) Nanoparticles/C	0.21	0.88	
20% Commercial Pt/C JM	0.30	0.26	

J_m: Mass Activity J_s: Specific Activity NA: not available

Table S3. Peak power density and lifetime of porous $Pt_{61}Te_8Rh_{31}$ NRs/C and commercial Pt/C for MEA catalysis under the self-breathing H_2-air fuel cell conditions.

Catalyst	**Loading of metal Pt (mg_{Pt} cm^{-2})**	**Peak power density ($W\ g^{-1}_{Pt}$)**	**Lifetime Peak power density loss**
commercial Pt/C	0.30	446.7	after 205 h, 89.6% loss
porous $Pt_{61}Te_8Rh_{31}$ NRs/C	0.17	1023.8	after 240 h, 35.7% loss

Table S4. MEA performances of porous $Pt_{61}Te_8Rh_{31}$ NRs/C and state-of-the-art Pt-based nanocatalysts as the cathodic catalysts from other published works in self-breathing PEMFC medium (room temperature and atmospheric pressure).

Catalyst (Anode Side ǁ Cathode Side)	**Peak Power Density ($mW\ cm^{-2}$)**	**Open Circuit Voltage in single cell (V)**	**Anodic/Cathodic Pt Loading Amounts (mg_{Pt} cm^{-2})**	**Ref.**
70% Commercial Pt/C (20% Nafion) ǁ 11.2% Porous $Pt_{61}Te_8Rh_{31}$ NRs/C (40% Nafion)	**174.05**	**0.921**	**0.50/0.17**	**This Work**
70% Commercial Pt/C (20% Nafion) ǁ 20% Commercial Pt/C (40% Nafion)	**134.00**	**0.917**	**0.50/0.30**	
30% Commercial PtRu/C ǁ 30% Commercial Pt/C with Flexible Porous CNT Membrane	145.2	~ 0.80	0.50/0.50	*ACS Nano* **2017**, *11*, 5982
Pt Nanoparticles/Graphene Nanosheets ǁ 70% Pt/C with Cone-Shaped Nafion Array-1.3 μm	139	~ 0.80	0.018/0.40	*J. Mater. Chem. A* **2020**, *8*, 5489
70% Commercial Pt/C ǁ 70% Commercial Pt/C with New GDL/Porous CNT Membrane	230	~ 0.95	0.50/0.50	*J. Mater. Chem. A* **2020**, *8*, 5986
70% Commercial Pt/C ǁ 70% Commercial Pt/C with Commercial GDL/Porous CNT Membrane	145	~ 0.79		
40% Commercial Pt/C ǁ 40% Commercial Pt/C with Circular Cathodic Opening Design	~ 275	~ 0.90	0.40/0.40	*Int. J. Hydrogen Energy* **2009**, *34*, 7761
40% Commercial Pt/C ǁ 40% Commercial Pt/C with Parallel Cathodic Opening Design	~ 210	~ 0.90		
Si Wafer-500 μm ǁ Pt Nanoparticles/Carbon Paper with 350 nm-sized Porous Si Surface	7.5	~ 0.90	0/0.38	*Microsyst. Technol.* **2017**, *23*, 3257
Si Wafer-500 μm ǁ Pt Nanoparticles/Carbon Paper with 5 μm-sized Porous Si Surface	5.5	~ 0.97		
60% Commercial Pt/C ǁ 60% Commercial Pt/C	~ 90	~ 0.92	0.10/0.15	*Science* **2019**, *366*, 850
60% Commercial Pt/C ǁ $Pt_{1.5}$Ni-BNCs/C	~ 110	~ 1.10		

Table S5. Peak power density and lifetime of porous $Pt_{61}Te_8Rh_{31}$ NRs/C and commercial Pt/C for MEA catalysis under the operating H_2-air/O_2 fuel cell conditions.

Catalyst		commercial Pt/C	porous $Pt_{61}Te_8Rh_{31}$ NRs/C
Loading of metal Pt (mg_{Pt} cm^{-2})		0.10	0.10
Peak power density in H_2/air medium ($mW\ cm^{-2}$)	50 kPa BP	/	682.8
	100 kPa BP	505.6	727.8
	150 kPa BP	555.4	743.4
Peak power density in H_2/O_2 medium ($mW\ cm^{-2}$)	50 kPa BP	/	1634.2
	100 kPa BP	1017.5	1851.0
	150 kPa BP	1338.8	1976.1
Peak power density loss in H_2/air medium	150 kPa BP	20.1%	13.2%
Peak power density loss in H_2/O_2 medium		25.7%	14.2%

Table S6. MEA performances of porous $Pt_{61}Te_8Rh_{31}$ NRs/C and state-of-the-art Pt-based nanocatalysts as the cathodic catalysts from recent 5 years-published works in H_2-O_2 PEMFC medium (specific pressure, 80 °C and 100% relative humidity).

Catalyst (Anode Side ǁ Cathode Side)	**Peak Power Density (mW cm^{-2})**	**Anodic/Cathodic Pt Loading Amounts (mg$_{Pt}$ cm^{-2})**	**Ref.**
20% Commercial Pt/C ǁ 11.2% Porous $Pt_{61}Te_8Rh_{31}$ NRs/C	**1976.1**	**0.10/0.10**	**This Work**
20% Commercial Pt/C ǁ 20% Commercial Pt/C	**1338.8**	**0.10/0.10**	
Pt-Based Catalyst ǁ Pt-Based Catalyst	> 1000	0.025/0.10	2025 U.S. DOE Target
Pt-Based Catalyst ǁ Pt-Ni Nanocages/C	1280	0.30/0.30	*Appl. Catal. B: Environ.* **2017**, *203*, 927
Pt-Based Catalyst ǁ Pt/C	1210		
20% Commercial Pt/C ǁ PtCo + Co@Graphene + Co-N_x-C_y	1050	0.35/0.033	*Science* **2018**, *362*, 1276
20% Commercial Pt/C ǁ Pt_3Co + Co@Graphene + Co/Zn-N_x-C_y	1420	0.35/0.035	
20% Commercial Pt/C ǁ Pt_3Co/ZC	740	0.35/0.043	
46% Commercial Pt/C ǁ Ga-PtNi Octahedra/C	~ 540	0.15/0.15	*Nano Lett.* **2018**, *18*, 2450
46% Commercial Pt/C ǁ PtNi Octahedra/C	~ 490		
46% Commercial Pt/C ǁ 46% Commercial Pt/C	~ 420		
20% Commercial Pt/C ǁ $L1_0$-W-PtCo/C	NA	0.10/0.11	*Angew. Chem. Int. Ed.* **2019**, *58*, 15471
20% Commercial Pt/C ǁ $Pt_{4.31}Ga$ Nanowires/C	~ 880	0.15/0.12	*J. Am. Chem. Soc.* **2019**, *141*, 18083
20% Commercial Pt/C ǁ 20% Commercial Pt/C	~ 720	0.15/0.14	
NA ǁ $L1_0$-CoPt/Pt Nanoparticles/C	NA	NA/0.105	*Joule* **2019**, *3*, 124
Pt/C ǁ oh-PtNi(Mo)/C	NA	0.10/0.10	*Nano Lett.* **2019**, *19*, 6876
Pt/C ǁ d-PtNi/C	NA		
Commercial PtRu/C ǁ PtCo@CNTs-MOF	1020	0.04/0.06	*J. Mater. Chem. A* **2019**, *7*, 19786
20% Commercial Pt/C ǁ $L1_0$-PtZn/Pt-C	2000	0.10/0.104	*Adv. Energy Mater.* **2020**, *10*, 2000179
20% Commercial Pt/C ǁ 20% Commercial Pt/C	~ 1200	0.10/0.16	
70% Commercial Pt/C ǁ 70% Commercial Pt/C with New GDL/Porous CNT Membrane	840	0.50/0.50	*J. Mater. Chem. A* **2020**, *8*, 5986
70% Commercial Pt/C ǁ 70% Commercial Pt/C with Commercial GDL/Porous CNT Membrane	634		
20% Commercial Pt/C ǁ PtFe/Pt-i-NPs/C	NA	0.08/0.02	*Science* **2021**, *374*, 459
20% Commercial Pt/C ǁ PtCo/Pt-i-NPs/C	NA		
20% Commercial Pt/C ǁ PtNi/Pt-i-NPs/C	NA		
20% Commercial Pt/C ǁ $PtCu_3$/Pt-i-NPs/C	NA		
20% Commercial Pt/C ǁ 20% Commercial Pt/C	NA	0.08/0.20	
Commercial Pt/C ǁ $L1_2$-Pt_3Co/FeN_4-C	NA	0.10/0.10	*Energy Environ. Sci.* **2021**, *14*, 4948
Commercial Pt/C ǁ Pt/FeN_4-C	NA		
60% Commercial Pt/C ǁ Sub-Pt_3Co-MC	~ 1750	0.20/0.20	*Proc. Natl. Acad. Sci. U.S.A.* **2021**, *118*, e2104026118
60% Commercial Pt/C ǁ 60% Commercial	~ 1100		

Pt/C			
20% Commercial Pt/C ‖ Pt_1@Pt/NBP	844	0.10/0.045	*ACS Catal.* **2021**, *11*, 466
20% Commercial Pt/C ‖ 20% Commercial Pt/C	1140	0.10/0.13	
40% Commercial Pt/C ‖ Ru-Pt_3Co Octahedra/C	1140	0.30/0.05	*Nano Lett.* **2021**, *21*, 6625
40% Commercial Pt/C ‖ Pt_3Co Octahedra/C	1164		
40% Commercial Pt/C ‖ 40% Commercial Pt/C	1033		
Pt-Based Catalyst ‖ PtCoNi@NCNTs	700	0.21/0.07	*Sci. Bull.* **2021**, *66*, 2207
Pt-Based Catalyst ‖ Commercial Pt/C	594	0.21/0.40	
46.4% Commercial Pt/C ‖ Pt-Fe-N-C	1080	0.10/0.015	*Nat. Catal.* **2022**, *5*, 503
46.4% Commercial Pt/C ‖ Pt-N-C	320	0.10/0.10	
Commercial Pt/C ‖ Commercial Pt/C-46.4%	1370	0.10/0.10	
40% Commercial Pt/C ‖ Pt_1Co_1-IMC@Pt/C	2300	0.10/0.20	*Energy Environ. Sci.* **2022**, *15*, 278
40% Commercial Pt/C ‖ 40% Commercial Pt/C	1990		
20% Commercial Pt/C ‖ PtCo@NGNS	860	0.10/0.10	*Angew. Chem. Int. Ed.* **2022**, *61*, e202115835
NA ‖ $Pt_{78}Zn_{22}$ Nanocubes/KB	1449.5	NA/0.15	*Adv. Sci.* **2022**, *9*, 2200147
NA ‖ 20% Commercial Pt/C	1149		
30% Commercial Pt/C ‖ Pd@Pt_{3L} Nanoparticles/C	1261	0.099/0.152	*Nano Res.* **2022**, *15*, 1892
30% Commercial Pt/C ‖ 30% Commercial Pt/C	~ 1200	0.102/0.298	

The specific pressure for fuel cell measurements is as shown in corresponding references.

NA: not available

Table S7. EXAFS parameters of Pt foil, PtTe NRs/C, porous $Pt_{95}Te_5$ NRs/C, PtTeRh NRs/C with different compositions, and porous PtTeRh NRs/C with different compositions.

Sample	Bond type	CN	R (Å)	σ^2 (10^{-3}Å^2)	R-factor (%)
Pt foil	Pt-Pt	12	2.76 ± 0.01	4.4 ± 0.2	0.1
PtTe NRs/C	Pt-Te	2.9 ± 0.3	2.64 ± 0.02	8.8 ± 1.0	2.2
	Pt-Pt	8.3 ± 0.8	2.77 ± 0.02	10.6 ± 1.0	
$Pt_3Te_3Rh_1$ NRs/C	Pt-Te	2.0 ± 0.2	2.65 ± 0.02	5.2 ± 0.8	1.8
	Pt-Pt	5.5 ± 0.7	2.73 ± 0.02	8.5 ± 1.1	
$Pt_3Te_3Rh_2$ NRs/C	Pt-Te	2.4 ± 0.2	2.65 ± 0.01	6.1 ± 0.7	1.1
	Pt-Pt	6.7 ± 0.5	2.75 ± 0.02	8.2 ± 0.7	
$Pt_3Te_3Rh_3$ NRs/C	Pt-Te	2.5 ± 0.2	2.65 ± 0.01	5.9 ± 0.6	0.9
	Pt-Pt	6.9 ± 0.6	2.74 ± 0.02	9.2 ± 0.8	
porous $Pt_{95}Te_5$ NRs/C	Pt-Pt	9.1 ± 0.6	2.75 ± 0.01	6.2 ± 0.4	0.7
porous $Pt_{69}Te_7Rh_{24}$ NRs/C	Pt-Rh	0.7 ± 0.3	2.68 ± 0.02	4.6 ± 2.3	0.6
	Pt-Pt	9.1 ± 0.5	2.75 ± 0.01	6.9 ± 0.4	
porous $Pt_{61}Te_8Rh_{31}$ NRs/C	Pt-Rh	0.8 ± 0.2	2.70 ± 0.02	1.8 ± 1.2	0.9
	Pt-Pt	7.1 ± 0.5	2.73 ± 0.01	5.8 ± 0.6	
porous $Pt_{62}Te_{15}Rh_{23}$ NRs/C	Pt-Rh	1.6 ± 0.2	2.71 ± 0.01	2.5 ± 0.8	1.4
	Pt-Pt	5.4 ± 0.5	2.72 ± 0.01	5.4 ± 0.8	

R, radial distance between absorber and backscatter atoms.

CN, coordination number.

σ^2, Debye-Waller factor value.

The passive electron reduction factor (S_0^2) was fixed to 0.81, as determined from Pt foil fitting.

R-factor (%) indicates the goodness of the fit.

Table S8. EXAFS parameters of Rh foil, PtTeRh NRs/C with different compositions, and porous PtTeRh NRs/C with different compositions.

Sample	Bond type	CN	R (Å)	σ^2 (10^{-3}Å^2)	R-factor (%)
Rh foil	Rh-Rh	12	2.69 ± 0.01	3.9 ± 0.3	0.9
$Pt_3Te_3Rh_1$ NRs/C	Rh-Te	4.2 ± 0.2	2.58 ± 0.02	1.7 ± 0.7	1.5
	Rh-Pt	9.8 ± 0.4	2.72 ± 0.02	2.5 ± 0.5	
$Pt_3Te_3Rh_2$ NRs/C	Rh-Te	4.2 ± 0.4	2.52 ± 0.02	1.2 ± 1.2	2.0
	Rh-Pt	14.8 ± 1.1	2.68 ± 0.02	8.4 ± 1.3	
$Pt_3Te_3Rh_3$ NRs/C	Rh-Te	5.0 ± 0.2	2.53 ± 0.02	4.2 ± 2.5	1.3
	Rh-Pt	8.2 ± 0.3	2.68 ± 0.02	3.1 ± 2.4	
porous $Pt_{69}Te_7Rh_{24}$ NRs/C	Rh-Te	6.9 ± 0.3	2.63 ± 0.02	4.4 ± 1.3	0.7
	Rh-Pt	6.3 ± 0.3	2.72 ± 0.02	11.1 ± 1.9	
porous $Pt_{61}Te_8Rh_{31}$ NRs/C	Rh-Te	9.3 ± 0.6	2.71 ± 0.02	3.0 ± 0.7	2.1
	Rh-Pt	3.5 ± 0.3	2.73 ± 0.02	1.6 ± 1.0	
porous $Pt_{62}Te_{15}Rh_{23}$ NRs/C	Rh-Te	5.7 ± 0.4	2.69 ± 0.02	5.2 ± 2.6	0.9
	Rh-Pt	7.5 ± 0.3	2.73 ± 0.02	5.6 ± 1.4	

R, radial distance between absorber and backscatter atoms.

CN, coordination number.

σ^2, Debye-Waller factor value.

The passive electron reduction factor (S_0^2) was fixed to 0.56, as determined from Rh foil fitting.

R-factor (%) indicates the goodness of the fit.